Journal of Power Sources 277 (2015) 426–432

Contents lists available at ScienceDirect

Journal of Power Sources

journal homepage: www.elsevier.com/locate/jpowsour

Mn in misch-metal based superlattice metal hydride alloy – Part 1 structural, hydrogen storage and electrochemical properties

K. Young [a, *], D.F. Wong [a, b], L. Wang [a, b], J. Nei [a], T. Ouchi [a], S. Yasuoka [c]

[a] BASF Battery Materials-Ovonic, 2983 Waterview Drive, Rochester Hills, MI 48309, USA
[b] Department of Chemical Engineering and Materials Science, Wayne State University, MI 48202, USA
[c] FDK Twicell Co., Ltd., 307-2 Koyagimachi, Takasaki 370-0071, Gunma, Japan

HIGHLIGHTS

- The various properties of misch-metal superlattice alloys were studied.
- Mn partially substituting Ni promotes formation of AB_5 phase.
- Mn decreases hydrogen storage capacities and degrade the surface catalytic ability.
- Mn adversely affects the cycle stability and high rate dischargeability.
- Magnetic susceptibility confirmed the Ni in the surface oxide as catalyst.

ARTICLE INFO

Article history:
Received 8 September 2014
Received in revised form
7 October 2014
Accepted 12 October 2014
Available online 23 October 2014

Keywords:
Hydrogen absorbing materials
Transition metal alloys
Metal hydride electrode
Electrochemical reactions

ABSTRACT

The structural, gaseous phase hydrogen storage, and electrochemical properties of a series of Mn-modified misch-metal based superlattice metal hydride alloys were investigated in part one of this two-part series of papers. X-ray diffraction analysis showed that these alloys are all multi-phased compositions with different abundances of AB_2, AB_3, A_2B_7, AB_4, and AB_5 phases. Substitution of Ni in the B-site by Mn promotes AB_5 phase formation and decreases both gaseous phase and electrochemical capacities due to the reduction in the abundance of main hexagonal A_2B_7 phase. AC impedance and magnetic susceptibility measurement were employed to characterize the surface of Mn-free and Mn-modified alloys and show deterioration in surface catalytic ability as the Mn-content increases. Mn-modification adversely affected misch-metal based superlattice metal hydride alloy properties such as phase homogeneity, capacity, cycle stability, high-rate performance, and surface reaction.

1. Introduction

The advances in personal portable electronics and battery-powered/assisted vehicles depend on the development of higher energy storage batteries. In response to such demand, misch-metal based superlattice metal hydride (MH) alloys with higher energy density were developed and first employed by Sanyo to increase the charge retention and capacity of nickel/metal hydride (Ni/MH) rechargeable batteries [1–3]. Recent results show that the cycle life of Ni/MH batteries can be increased to 6000 cycles by utilizing these superlattice alloys [4]. Where conventional AB_5 and AB_2 MH alloys used in Ni/MH batteries contain single- ($LaNi_5$-based) or multi-phase (Laves phases-based) structures, respectively; superlattice MH alloys are composed of phases with alternating building blocks of A_2B_4 slab and different numbers of AB_5 slabs [5,6]. The stoichiometry of these phases ranges from B/A = 3 to 4 (AB_3, A_2B_7, A_5B_{19}, and AB_4). Academic publications reported for the superlattice alloy family tend to focus on La- and Nd-only alloys, for which we have summarized the research efforts in a separate review article [7]. While the misch-metal based superlattice MH alloys containing two or more different rare earth elements have good balance between cost and performance, they are more difficult to prepare due to phase segregation that cannot be resolved by annealing alone [8,9], and thus this type of MH alloy is not widely available on the market, especially outside Japan.

Mn is an indispensable element in conventional misch-metal based AB_5 MH alloys for maintaining cycle stability [10] and high-rate dischargeability (HRD) [11,12]. However, a superlattice alloy without any Mn was shown to improve charge retention characteristics without significant sacrifices in cycle stability and HRD [3].

* Corresponding author. Tel.: +1 248 293 7000; fax: +1 248 299 4520.
E-mail address: kwo.young@basf.com (K. Young).

http://dx.doi.org/10.1016/j.jpowsour.2014.10.093
0378-7753/

Table 1
Design compositions (in bold) and ICP results in at%.

		Mm	Mg	Ni	Al	Mn	Fe	Mg/A	B/A
F1	**Design**	**19.3**	**3.9**	**72.8**	**4.0**	**0.0**	**0.0**	**0.17**	**3.31**
	ICP	19.0	3.9	72.5	4.6	N.D.	N.D.	0.17	3.37
F2	**Design**	**19.3**	**3.9**	**70.5**	**4.0**	**2.3**	**0.0**	**0.17**	**3.31**
	ICP	19.1	3.7	70.8	4.0	2.3	N.D.	0.16	3.38
F3	**Design**	**19.3**	**3.9**	**68.1**	**4.0**	**4.7**	**0.0**	**0.17**	**3.31**
	ICP	19.2	3.7	68.3	3.9	4.7	N.D.	0.16	3.36
F4	**Design**	**19.3**	**3.9**	**65.8**	**4.0**	**7.0**	**0.0**	**0.17**	**3.31**
	ICP	19.3	4.0	65.4	4.2	7.0	0.1	0.17	3.29
F5	**Design**	**19.3**	**3.9**	**63.5**	**4.0**	**9.3**	**0.0**	**0.17**	**3.31**
	ICP	19.2	3.9	63.5	4.0	9.4	N.D.	0.17	3.33

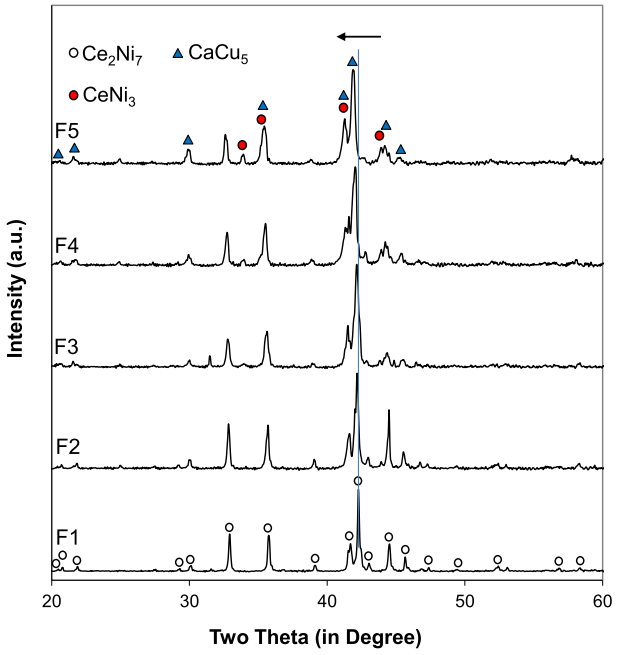

Fig. 1. XRD patterns using Cu-K_α as the radiation source for alloys F1–F5. The vertical line indicates the shift of Ce_2Ni_7 peak to lower angles as the Mn-content increases.

A systematic study of the effect of Mn in superlattice alloys is therefore of interest and is presented in this two-part publication. The properties of Mn-free and Mn-modified alloys in powder form are discussed in Part 1, and in Part 2, the performances and failure modes of Ni/MH batteries using these alloys are presented and compared to batteries using conventional AB_5 MH alloys [13].

2. Experimental setup

Induction melting from elementary raw materials was performed by Japan Metals and Chemicals Co., Ltd. Ingots were mechanically ground to −200-mesh powder. The chemical composition of each sample was examined by a Varian *Liberty* 100 inductively-coupled plasma (ICP) system. A Philips *X'Pert Pro* x-ray diffractometer (XRD) was used to study the microstructure, and a JEOL-*JSM6320F* scanning electron microscope (SEM) with energy dispersive spectroscopy (EDS) capability was used to study the phase distribution and composition. Pressure-concentration-temperature (PCT) characteristics of each sample were measured using a Suzuki-Shokan multi-channel PCT system. Half-cell testing was performed using an Arbin Instruments BT4+ Portable Battery Test System. AC impedance measurement was conducted using a Solartron 1250 Frequency Response Analyzer with sine wave amplitude of 10 mV and frequency range of 0.5 mHz–10 kHz. Prior to the measurement, the electrode was subjected to one full charge/discharge cycle at 0.1C rate using a Solartron 1470 Cell Test galvanostat, discharged to 80% state-of-charge, and then cooled down to −40 °C. Magnetic susceptibility was measured using a Digital Measurement Systems Model 880 vibrating sample magnetometer.

3. Results and discussion

Five alloys ($Mm_{0.83}Mg_{0.17}Ni_{3.14-x}Al_{0.17}Mn_x$, $x = 0$, 0.1, 0.2, 0.3, and 0.4) were prepared, and their design compositions are listed in Table 1. The Mn-content varies from 0 to 9.3 at% at the expense of Ni. A design B/A ratio of 3.31 is applied to all alloys in this study. ICP results of ingots (shown in the same table) are very close to the design compositions. During melting, extra Mg was added to compensate for loss due to evaporation, and the ICP results confirm that the average Mg-content in each ingot is adequate. A very small amount of Fe pick-up from the steel mold is found in one of the ingots (F4).

3.1. XRD analysis

XRD patterns of the five samples (F1–F5) are shown in Fig. 1. All patterns show a multi-phase natured composition of AB_2, AB_5, and superlattice phases (AB_3, A_2B_7, and A_5B_{19}) in various degrees. Two crystal structures, rhombohedral and hexagonal, exist for AB_3, A_2B_7, and A_5B_{19} compositions. Jade 9 software was utilized to calculate the phase abundances while the overlapping of peaks from different phase is very severe, and the results are listed in Table 2. The Mn-free alloy, F1, has a main phase of hexagonal Ce_2Ni_7 structure (62.0%) and four secondary phases of hexagonal Pr_5Co_{19} (19.2%), rhombohedral Ce_5Co_{19} (9.1%), rhombohedral $PuNi_3$ (7.7%), and hexagonal $CeNi_3$ (2.0%) structures. As the Mn-content increases, the following trends can be observed:

1. The main Ce_2Ni_7 phase abundance decreases and the unit cell expands as indicated in the peak shift marked by the arrow in Fig. 1.
2. The $CeNi_3$ phase abundance increases.
3. Both $PuNi_3$ and Pr_5Co_{19} phase abundances decrease.
4. Rhombohedral Pr_2Ni_7 phase appears in alloys with higher Mn-content (F4 and F5).
5. $CaCu_5$ phase appears.

Table 2
Lattice constants *a* and *c*, *c*/*a* ratio, and crystallite size of the main Ce_2Ni_7 phase (estimated from the (109) peak), and phase abundances in wt.% calculated from XRD analysis of alloys F1–F5. R: rhombohedral, H: hexagonal.

	a of Ce_2Ni_7 (Å)	*c* of Ce_2Ni_7 (Å)	*c*/*a* ratio of Ce_2Ni_7	Crystallite size of Ce_2Ni_7 (Å)	$MgZn_2$ (H) abundance (%)	$CeNi_3$ (H) abundance (%)	$PuNi_3$ (R) abundance (%)	Ce_2Ni_7 (H) abundance (%)	Pr_2Ni_7 (R) abundance (%)	Pr_5Co_{19} (H) abundance (%)	Ce_5Co_{19} (R) abundance (%)	$CaCu_5$ (H) abundance (%)	Nd_2O_3 abundance (%)
F1	5.0216	24.4203	4.863	913	0.0	2.0	7.7	62.0	0.0	19.2	9.1	0.0	0.0
F2	5.0313	24.4507	4.860	633	0.0	19.5	4.1	45.2	0.0	11.0	5.8	14.4	0.0
F3	5.0374	24.4643	4.857	477	0.0	23.1	0.0	44.4	0.0	0.0	21.3	10.8	0.4
F4	5.0492	24.5062	4.853	317	1.9	26.3	0.0	48.3	11.5	0.0	0.0	11.9	0.0
F5	5.0564	24.5216	4.850	290	0.0	32.2	0.0	39.6	11.5	0.0	0.0	16.7	0.0